

# COMPUTATIONAL MODELING AND SIMULATION OF METAL PLASMA GENERATION BETWEEN CYLINDRICAL ELECTRODES USING PULSED POWER

K. Kim,<sup>1</sup> H.S. Kwak<sup>1</sup> and J.Y. Park<sup>2</sup>

<sup>1</sup>Department of Mechanical System Engineering, Kumoh National Institute of Technology

<sup>2</sup>Department of Mechatronics, Kumoh National Institute of Technology

## 펄스파워를 이용한 실린더형 전극간 금속 플라즈마 생성현상의 전산유동해석

김 경 진,<sup>1</sup> 곽 호 상,<sup>1</sup> 박 중 윤<sup>2</sup>

<sup>1</sup>금오공과대학교 기계시스템공학과

<sup>2</sup>금오공과대학교 기전공학과

*This computational study features the transient compressible and inviscid flow analysis on a metallic plasma discharge from the opposing composite electrodes which is subjected to pulsed electric power. The computations have been performed using the flux corrected transport algorithm on the axisymmetric two-dimensional domain of electrode gap and outer space along with the calculation of plasma compositions and thermophysical properties such as plasma electrical conductivity. The mass ablation from aluminum electrode surfaces are modeled with radiative flux from plasma column experiencing intense Joule heating. The computational results shows the highly ionized and highly under-expanded supersonic plasma discharge with strong shock structure of Mach disk and blast wave propagation, which is very similar to muzzle blast or axial plasma jet flows. Also, the geometrical effects of composite electrodes are investigated to compare the amount of mass ablation and penetration depth of plasma discharge.*

**Key Words :** 플라즈마 생성(Plasma Generation), 펄스파워(Pulsed Power), 실린더형 전극(Cylindrical Electrode), 전산유체역학(CFD)

### 1. Introduction

A metallic plasma discharge of high temperature and density using the high power pulsed electrical discharge can be useful in many technical areas such as production of novel materials and nanoparticles or the thermal plasma spray coatings. Derived from the concept of electrothermal-chemical (ETC) gun, which has been originally developed to improve the solid propellant combustion for the acceleration of the projectile[1,2], there have been considerable research efforts to produce pulsed

metallic plasma discharge using this device. The ETC gun employs the high power discharge of electrical energy to vaporize the solid materials of capillary bore and electrodes. The ionized vapor of ablated material forms a high density plasma for the duration of a high current discharge and the plasma discharge exits the open end of bore to create the external plasma jet with complex shock structures.

By using the modified ETC gun, Peterson[3] studied the potentials of pulsed arc discharge as an efficient source of the metal plasma vapor spray, while Kim[4,5] could manufacture a variety of nanocrystalline metallic and ceramic powders with the pulsed plasma jet discharged into the background gas in the reaction chamber. Also, Kim[6,7] carried out computational studies on pulsed plasma jet into the open-air.

Although ETC gun could be an efficient method in

Received: November 18, 2014, Revised: December 15, 2014,

Accepted: December 15, 2014.

\* Corresponding author, E-mail: jypark@kumoh.ac.kr

DOI <http://dx.doi.org/10.6112/kscfe.2014.19.4.068>

© KSCFE 2014

producing metallic plasmas, there are several disadvantages such as possible contamination due to polycarbonate bore material or necessity of fuse wire between electrodes. In order to address those technical difficulties, the production of pulsed metallic plasma using the opposing electrodes has been proposed and in use for the continuous firing of pulsed plasma discharge[8].

This paper presents the computational study on the transient plasma discharge from the operation of pulsed plasma arc between the opposing electrodes in order to better understand the expansion of plasma discharge as well as the prediction of metallic electrode ablation by pulsed electrical power.

## 2. Computational Models and Methods

### 2.1 Electrode Setup for Pulsed Plasma Discharge

Fig. 1(a) illustrates the concept of metallic plasma generation between the opposing electrodes and it is operated by a pulse forming network (PFN), which consists of the capacitor banks, inductors, resistors, and the ignition switches. Once the electrical energy stored in the capacitor bank of PFN is discharged into the electrodes, a current path between anode and cathode are expected to be established, if the gap distance between the electrodes is small enough. Then, the ablated metallic materials from the electrode surfaces is subsequently vaporized and ionized due to intense Joule heating. The resulting plasma rapidly expands from the electrode gap into the exterior space.

In order to establish the stable electric arc at the center of electrodes, the composite form of the electrodes is used in this study, as shown in Fig. 1(b). The composite electrodes consist of cylindrical rod (diameter of  $D_e = 3/16$  in. = 4.7625 mm) at the center, where the pulsed electrical current passes through, and annular cylinder (outer diameter of  $D_o = 3/4$  in. = 19.05 mm). Both regions of electrode are made of aluminum and they are separated by the thin electrically insulating plastic material. The gap distance between two electrodes ( $d$ ) is set to be  $1/8$  in. or 3.175 mm.

### 2.2 Plasma Discharge Model

For the computational simulation of expanding inviscid flow of aluminum plasma generated from the opposing composite electrodes, the following transient governing equations for the conservation of mass, momentum, and energy transport in radial and axial directions can be

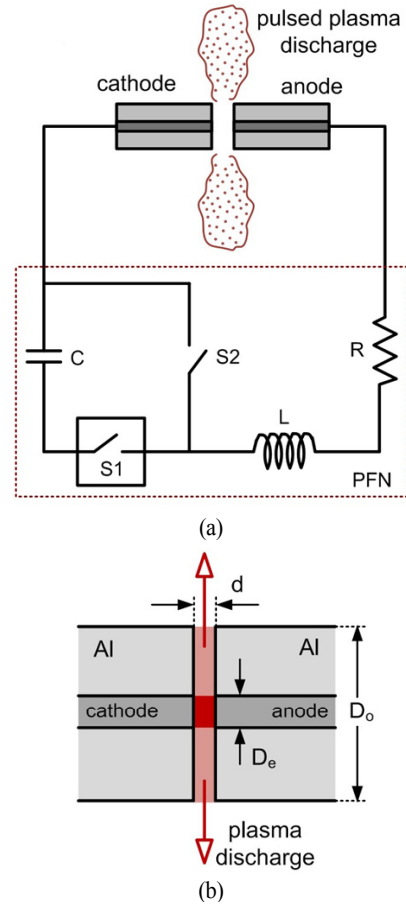


Fig. 1 Schematic (a) and geometry (b) of plasma discharge between cylindrical electrodes with pulse forming network

employed[7]:

$$\frac{\partial \rho}{\partial t} + \frac{1}{r} \frac{\partial}{\partial r}(r \rho u_r) + \frac{\partial}{\partial z}(\rho u_z) = \dot{\rho}_a \quad (1)$$

$$\frac{\partial \rho u_r}{\partial t} + \frac{1}{r} \frac{\partial}{\partial r}(r \rho u_r^2) + \frac{\partial}{\partial z}(\rho u_r u_z) = - \frac{\partial P}{\partial r} \quad (2)$$

$$\frac{\partial \rho u_z}{\partial t} + \frac{1}{r} \frac{\partial}{\partial r}(r \rho u_r u_z) + \frac{\partial}{\partial z}(\rho u_z^2) = - \frac{\partial P}{\partial z} \quad (3)$$

$$\frac{\partial \rho \epsilon}{\partial t} + \frac{1}{r} \frac{\partial}{\partial r}(r \rho u_r \epsilon) + \frac{\partial}{\partial z}(\rho u_z \epsilon) = \frac{J^2}{\sigma} \quad (4)$$

$$\epsilon = e + \frac{1}{2}(u_r^2 + u_z^2) + \frac{P}{\rho} \quad (5)$$

where  $P$ ,  $\rho$ ,  $u_r$ ,  $u_z$ , and  $e$  are the pressure, mass

density, radial and axial velocity components, and the specific internal energy, respectively. In Eq. (4), the right-hand side term represents the Joule heating in the volume only between inner rods of electrodes ( $\pi D_e^2 d/4$ ), and  $J (= 4I/\pi D_e^2)$  and  $\sigma$  are current density and plasma electrical conductivity, respectively. The plasma specific internal energy includes thermal energy, electronic energy, and chemical energy components such as

$$e = 3(1 + \alpha)kT/2\bar{m} + e_{el} + e_{chem} \quad (6)$$

where  $T$ ,  $\alpha$ ,  $k$ , and  $\bar{m}$  are temperature, degree of ionization, Boltzmann constant, and average atomic mass of neutrals and ions, respectively. Also, it is assumed that the plasma obeys the following ideal gas approximation.

$$P = (1 + \alpha)\rho kT/\bar{m} \quad (7)$$

The mass ablation from two electrodes is approximated as the volumetric phenomena, not being treated as boundary condition. The source term  $\dot{\rho}_a$  in Eq. (1) is the mass ablation density rate in the volume of  $\pi D_e^2 d/4$ . Similarly as in the previous studies[6,7], the mass ablation is modeled by equating the radiative flux from the plasma column to electrode surfaces ( $2 \times \pi D_e^2/4$ ) and total energy of the ablated material inside the gap, and it is given by

$$\dot{\rho}_a = \frac{2f\sigma_{sb}T^4}{d\epsilon} \quad (8)$$

where  $\sigma_{sb}$  is the Stefan-Boltzmann constant. The factor  $f$  represents the deviation from blackbody radiative heating and it is shown to be close to unity when compared with experiments[6]. Thus, this study will simply assume it to be unity. Note that the ablation of thin insulating material is neglected.

The computational method used in this study for solving governing equations of Eq. (1)-(4) is based on LCPFCT scheme[9] and it employs the one-dimensional flux-corrected transport (FCT) algorithm with fourth-order phase accuracy. This scheme has been proven to be highly accurate and efficient especially in resolving steep gradients. Also, it can be easily extended to the two-dimensional cases by time step splitting in each spatial coordinate direction. Thus, a set of the aforementioned governing equations is separated into two sets of one-dimensional conservation equations for radial

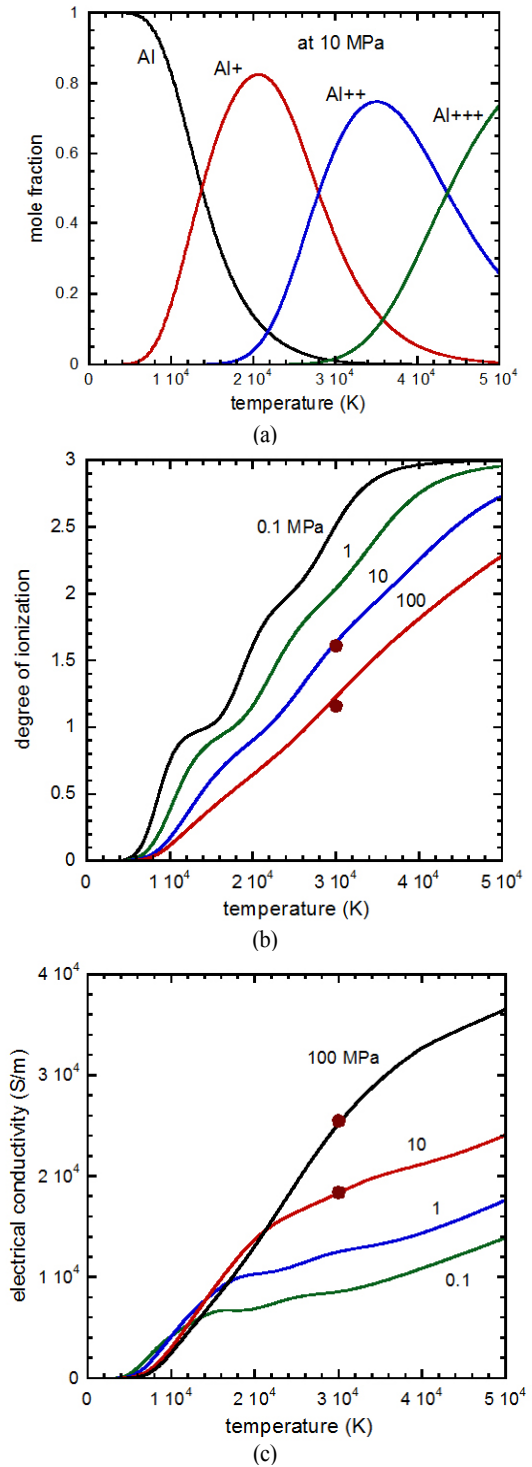


Fig. 2 Mole fraction of heavy species at 10 MPa (a), degree of ionization (b), and electrical conductivity (c) for aluminum plasma. Symbols are from Batteh et al.[12]

and axial coordinates and they are readily subjected to successive integration through both directions at each time step. The integrating time step is determined by the CFL condition.

**2.3 Plasma Property Evaluation**

Due to intense Joule heating, the ablated mass from electrodes could be partially or fully ionized and becomes metal plasma. Assuming that the plasma flow is in local ionization equilibrium, the plasma compositions are determined by employing the Saha equations:

$$\frac{n_e n_{i+1}}{n_i} = 2 \frac{Q_{i+1}}{Q_i} \left( \frac{2\pi m_e k T}{h^2} \right)^{3/2} \exp\left( - \frac{I_i - \Delta I_i}{k T} \right) \quad (9)$$

The subscripts *i* and *i+1* indicates a certain heavy species and its next ionization level, while *n<sub>e</sub>*, *m<sub>e</sub>*, *h* are the electron number density, electron mass, and Planck constant, respectively. The partition functions *Q<sub>i</sub>* are determined by considering the degeneracy and energy of electronic excitation level. The term  $\Delta I_i$  represents the lowering in the ionization energy of heavy species *I<sub>i</sub>* due to nonideal plasma behavior[10].

It is important to evaluate electrical conductivity of plasma with reasonable accuracy and it is determined by considering the electron collisions with both neutral atoms and ions such as[11]

$$\sigma = \frac{n_e e^2}{m_e (\bar{\nu}_{en} + \bar{\nu}_{ei})} \quad (10)$$

where  $\bar{\nu}_{en}$  and  $\bar{\nu}_{ei}$  are the electron-neutral and electron-ion collision frequencies and *e* is the electron charge. Detailed calculation procedures for thermodynamic and transport properties of plasma can be found in references[6,10,11].

Here, up to three ionization levels for aluminum species are considered (Al, Al<sup>+</sup>, Al<sup>++</sup>, Al<sup>+++</sup>), as Fig. 2(a) shows the effects of temperature on the molar composition of aluminum heavy species at 10 MPa. Fig. 2(b) and 2(c) show the degree ionization and electrical conductivity up to temperature of 50,000 K for the pressure levels from 0.1 to 100 MPa. Note that the symbols in those figures represent the corresponding computational results at 30,000 K (for 100 and 1,000 atm) by Batteh et al.[12] and they are in good agreement with the present plasma property calculations.

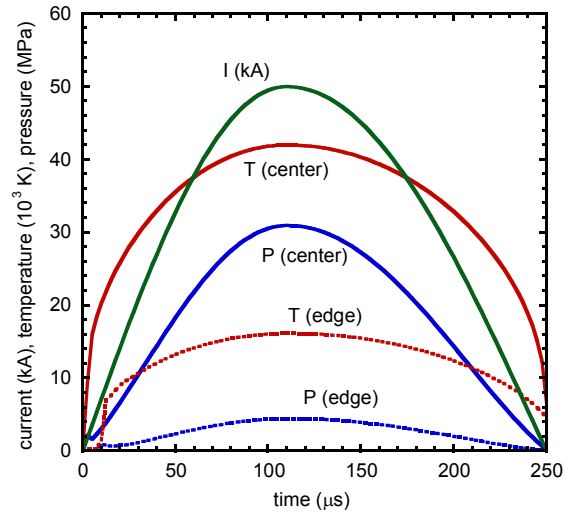


Fig. 3 Temporal change of electrical current and plasma conditions at the center and edge of electrode gap

**3. Results and Discussion**

The computational flow analysis for expanding aluminum plasma discharge from the composite electrodes has been performed with two-dimensional axisymmetric domain, which includes only the half of the gap between electrodes and the open-air region due to symmetry along radial coordinate. The size of computational domain is 98.43 and 80.69 mm in radial and axial directions, respectively, and it should be large enough to accommodate the outgoing plasma penetration. The total number of grid points is approximately 113,000, while the structured grids are more finely placed around the region near electrode gap to resolve the steep gradients. The initial condition is the quiescent air at the standard atmospheric conditions.

Temporal traces of electrical current from capacitor bank of the pulse forming network, which acts between two electrodes, are prescribed as shown in Fig. 3 using the measured profile from the experiments. The pulse duration is 250 μs and peak current of 50 kA occurs approximately at time of 110 μs. The time integration has been carried out up to 300 μs.

The detailed flow characteristics of radially expanding metal plasma discharge from the electrode gap can be examined in Fig. 4, which captures the spatial distributions of Mach number and temperature at time of 100 μs. This transient flowfield exhibits the typical shock structures of

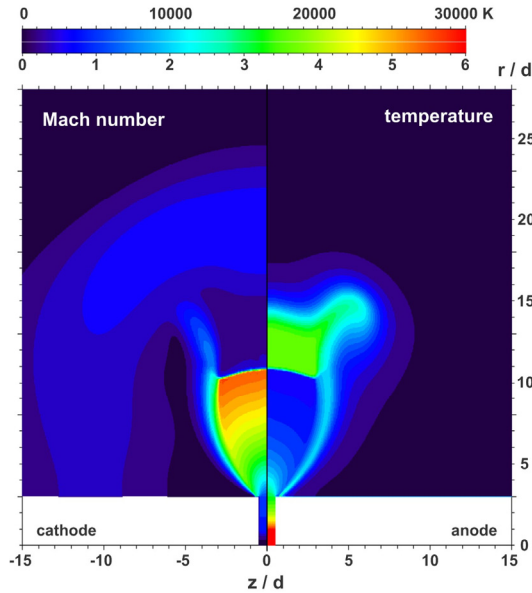


Fig. 4 Mach number and temperature distributions of radial plasma discharge at time of 100  $\mu$ s

highly under-expanded supersonic jet in radial direction which is quite similar to impulsive muzzle blast in gun firings[13,14] or axial plasma jet discharge by pulsed electrical power in ETC gun operations[7]. It features the strong shock formation of advancing and retreating Mach disk along with barrel shock on the side as well as spherical propagation of the blast wave.

Transient changes of plasma temperature and pressure at the center and edge of electrode gap are shown in Fig. 3. Because of the intense Joule heating between the electrodes, plasma temperature could exceed 40,000 K at the center with extremely high pressure. When the plasma exits the electrode gap, plasma temperature and pressure decrease substantially due to radial expansion and loss of energy to metal ablation. Such a extreme plasma condition in the electrode gap leads to the strong plasma expansion and shock formation into the open space outside the electrode gap.

Fig. 5 shows the spatial change of Mach number, temperature, pressure, and mass density of plasma discharge along the radial coordinate (at  $z/d = 0$ ) for the time of 100  $\mu$ s. Up to  $r/d = (D_o/2)/d = 3$  (exit location from electrode gap space), significant decrease of temperature and plasma can be observed, while the mass density remains almost constant due to continuous mass addition from metal surface ablation. Note that Mach number reaches unity around this location and it indicates

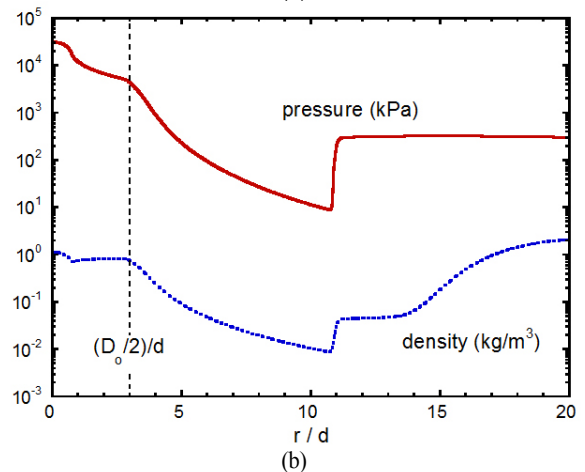
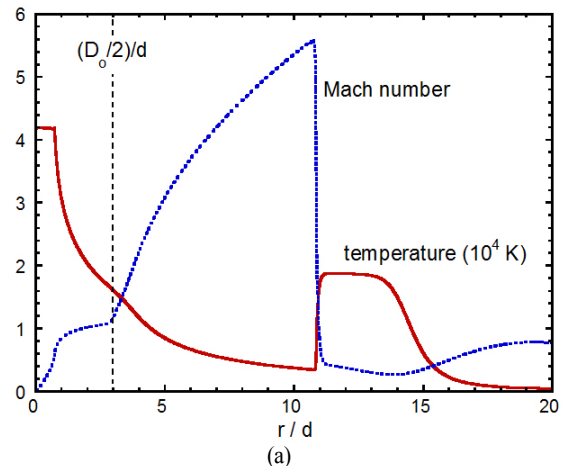


Fig. 5 Radial distributions of Mach number, temperature (a), pressure, and density (b) in plasma discharge at time of 100  $\mu$ s

the choking of plasma flow. In the unbounded open space ( $r/d > 3$ ), plasma discharge rapidly expands and forms the shock structure. Mach disk location can be clearly identified approximately at  $r/d = 11$ .

In addition to the base case of composite electrodes, two more cases are investigated to study the effects of varying electrode size. The first is with larger cylindrical rod at the center ( $D_e = \sqrt{2} \times 3/16$  in.), while the outer diameter of annular cylindrical rod is unchanged ( $D_o = 3/4$  in.). Therefore, the cross-section where the electrical current passes is doubled but the surface area subjected to plasma ablation remains the same. In the second case, the diameter of cylindrical rod at the center is unchanged ( $D_e = 3/16$  in.) but the overall cross-section of composite electrode is doubled ( $D_o = \sqrt{2} \times 3/4$  in.). Note that the

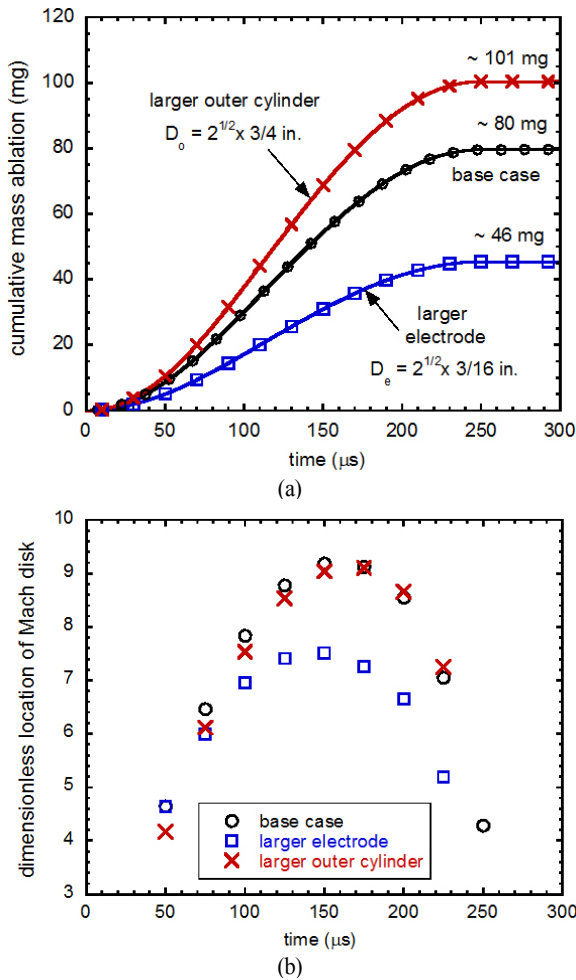


Fig. 6 Cumulative mass ablation from electrode surface (a) and transient radial location of Mach disk (b)

rest of operating conditions are identical such as pulsed form of electrical current or gap distance.

Fig. 6(a) shows the cumulative mass of ablated aluminum from the electrode surfaces through the pulse duration which can be evaluated by volume integration of mass ablation density rate inside electrode gap. While the amount of mass ablation is approximately 80 mg, it increases to 101 mg by enlarging the overall size of composite electrode. However, the enlarging inner electrode size effectively decreases the ablated mass due to diminished intensity of Joule heating. The penetration of metal plasma discharge can be compared among those three cases by examining transient location of Mach disk in Fig. 6(b). As expected, the case of larger electrode could be less effective than the other cases of electrode

geometry.

#### 4. Conclusions

In this computational study, the pulsed plasma generation and discharge from the opposing composite electrodes are numerically simulated with the volumetric model of mass ablation. The numerical results shows that, due to intense Joule heating in the electrode gap, ablated mass from aluminum electrode surface become fully ionized and expands outside the gap forming advancing and retreating Mach disk and other shock structures. In designing the composite electrodes, adjusting the diameters in electrode geometry can adjust the amount of mass ablation as well as the penetration of plasma discharge.

#### Acknowledgements

This research was supported by Research Fund, Kumoh National Institute of Technology.

#### References

- [1] 2002, Nusca, M.J., McQuaid, M.J. and Anderson, W.R., "Numerical Model of the Plasma Jet Generated by an Electrothermal-Chemical Igniter," *J. Thermophys. Heat Transfer*, Vol.16, pp.157-160.
- [2] 2006, Keidar, M. and Boyd, I.D., "Ablation Study in the Capillary Discharge of an Electrothermal Gun," *J. Appl. Phys.*, Vol.99, pp.053301-1-7.
- [3] 1997, Peterson, D.R., "Design and Operation of the Electrogun, an Electrothermal Gun for Producing Metal and Carbon Plasma Jets," *IEEE Trans. Magn.*, Vol.33, pp.373-378.
- [4] 2005, Kim, K., "Plasma Synthesis and Characterization of Nanocrystalline Aluminum Nitride Particles by Aluminum Plasma Jet Discharge," *J. Cryst. Growth*, Vol.283, pp.540-546.
- [5] 2008, Kim, K., "High Energy Pulsed Plasma Arc Synthesis and Material Characteristics of Nanosized Aluminum Powder," *Met. Mater. Int.*, Vol.14, pp.707-711.
- [6] 2003, Kim, K., "Time-Dependent One-Dimensional Modeling of Pulsed Plasma Discharge in a Capillary Plasma Device," *IEEE Trans. Plasma Sci.*, Vol.31, pp.729-735.
- [7] 2008, Kim, K., "Transient Flowfield Characteristics of

- Polycarbonate Plasma Discharge from Pulse-Powered Electrothermal Gun Operation," *J. Therm. Spray Technol.*, Vol.17, pp.517-524.
- [8] 2002, Schroder, K., Wilson, D.E., Kim, K. and Elliott, H.E., "Characterization of Metallic and Metal Oxide Nanoparticles Produced by Electrothermal-Chemical Synthesis," *MRS Proceedings*, Vol.744, pp.389-394.
- [9] 1993, Boris, J.P., Landsberg, A.M., Oran, E.S. and Gardner, J.H., "LCPFCT - Flux-Corrected Transport Algorithm for Solving Generalized Continuity Equations," *NRL MR 6410-93-7192*, Naval Research Laboratory, Washington, D.C.
- [10] 1992, Powell, J. and Zielinski, A., "Theory and Experiment for an Ablating-Capillary Discharge and Applications to Electrothermal-Chemical Guns," *BRL-TR-3355*, U.S. Army Ballistic Research Laboratory, Aberdeen Proving Ground.
- [11] 1987, Liebermann, R.W. and Zollweg, R.J., "Electrical Conductivity of Nonideal Plasmas," *J. Appl. Phys.*, Vol.62, pp.3621-3627.
- [12] 1995, Batteh, J., Powell, J., Sink, D. and Thornhill, L., "A Methodology for Computing Thermodynamic and Transport Properties of Plasma Mixtures in ETC Injectors," *IEEE Trans. Magn.*, Vol.31, pp.388-393.
- [13] 1975, Schmidt, E.M. and Shear, D.D., "Optical Measurements of Muzzle Blast," *AIAA J.*, Vol.13, pp.1086-1091.
- [14] 1975, Erdos, J.I. and Del Giudice, P.D., "Calculation of Muzzle Blast Flowfields." *AIAA J.*, Vol.13, pp.1048-1055.